

Mini-Slot-Assisted Short Packet URLLC: Differential or Coherent Detection?

Canjian Zheng, Fu-Chun Zheng, *Senior Member, IEEE*, Jingjing Luo, *Member, IEEE*, Pengcheng Zhu, *Member, IEEE*, Xiaohu You, *Fellow, IEEE* and Daquan Feng, *Member, IEEE*

Abstract—One of the primary challenges in short packet ultra-reliable and low-latency communications (URLLC) is to achieve reliable channel estimation and data detection while minimizing the impact on latency performance. Given the small packet size in mini-slot-assisted URLLC, relying solely on pilot-based coherent detection is almost impossible to meet the seemingly contradictory requirements of high channel estimation accuracy, high reliability, low training overhead, and low latency. In this paper, we explore differential modulation both in the frequency domain and in the time domain, and propose adopting an adaptive approach that integrates both differential and coherent detection to achieve mini-slot-assisted short packet URLLC, striking a balance among training overhead, system performance, and computational complexity. Specifically, differential (especially in the frequency domain) and coherent detection schemes can be dynamically activated based on application scenarios, channel statistics, information payloads, mini-slot deployment options, and service requirements. Furthermore, we derive the block error rate (BLER) for pilot-based, frequency domain, and time domain differential OFDM using non-asymptotic information-theoretic bounds. Simulation results validate the feasibility and effectiveness of adaptive differential and coherent detection.

Index Terms—URLLC, short packet transmission, frequency domain differential modulation, time domain differential modulation, mini-slot, OFDM, coherent detection and differential detection.

I. INTRODUCTION

A. Background

Ultra-reliable and low-latency communications (URLLC) is a primary use case in the 5th generation (5G) wireless networks, facilitating various mission-critical applications such as factory automation, remote surgery, tactile internet, and autonomous driving. To support these applications, the 3rd generation partnership project (3GPP) has specified typical URLLC requirements of 1 ms physical layer latency and 99.999% (5-nines) reliability for 5G networks [1], [2]. As emerging services place increasingly stringent demands on the network performance, it is further expected that the physical layer latency and reliability requirements for enhanced URLLC in the forthcoming B5G and 6G networks could reach 0.1 ms levels and 99.99999% (7-nines), respectively [3]–[5].

To satisfy such stringent performance requirements in URLLC, 3GPP has introduced the novel feature of mini-slot for 5G networks [6]. Specifically, the mini-slot employs a group of 2, 4, or 7 orthogonal frequency-division multiplexing (OFDM) symbols as a basic unit for data scheduling and resource allocation. In contrast, the smallest scheduling unit for the other two primary use cases in 5G networks (i.e., enhanced mobile broadband (eMBB) and massive machine-type

communications (mMTC)) is a conventional slot occupying 12 or 14 OFDM symbols [7]. Unlike the conventional slot, where packets arriving within a slot must wait until the end of the slot for transmission, the mini-slot-assisted data transmission with a finer time domain partitioning can start at any OFDM symbol without waiting for a slot boundary [8]. Therefore, the mini-slot feature is particularly suitable for short sized packets containing tens to hundreds of bytes to enable rapid data delivery and transmission responsiveness.

B. Motivations

In mini-slot-assisted short packet transmission (SPT), using pilot symbols, also known as demodulation reference signals in 5G networks, to acquire accurate channel state information (CSI) is essential for coherent detection. However, the pilot overhead for channel estimation can consume a considerable portion of the valuable time, bandwidth and power resources in mini-slot-assisted SPT [9]. Figs.1(a-d) illustrate the pilot patterns specified in 3GPP Release 18 for coherent detected short packet URLLC utilizing 2, 4 and 7 OFDM symbol units¹. As shown in Fig.1(a), up to 25% of the total packet of a 2 OFDM symbol unit is allocated to pilot symbols for channel estimation regardless of mobility scenarios, which is expensive for short packet URLLC and impairs significantly the latency performance. On the other hand, reducing the pilot percentage in mini-slot-assisted SPT may lead to a deterioration in channel estimation accuracy, severely degrading the performance of coherent detection, especially in high mobility scenarios where a fading channel can fluctuate rapidly.

To simultaneously mitigate the costly channel estimation overhead and avoid the significant performance degradation in mini-slot-assisted SPT, one promising solution is to apply non-coherent detection, which does not require CSI [10]. Differential modulation (DM) has therefore emerged as an appealing non-coherent detection scheme over the years for various wireless communications systems due to its simple transceiver structure and low complexity (e.g. [10] and [11]). In DM, the transmitter maps the information into the phase difference between consecutive symbols, while the receiver recovers the

¹In order to support different service scenarios and use cases in mini-slot-assisted SPT, 3GPP Release 18 defines a fixed and suboptimal deployment of pilot symbols. Specifically, to allow immediate channel estimation and coherent detection as soon as data symbols are received, pilots are always placed at equally spaced subcarriers of the first OFDM symbol in the mini-slot. Furthermore, for high mobility scenarios, additional pilots can be deployed in the middle of the mini-slot of greater than 4 OFDM symbols to improve the channel estimation performance, as shown in Fig.1(d).

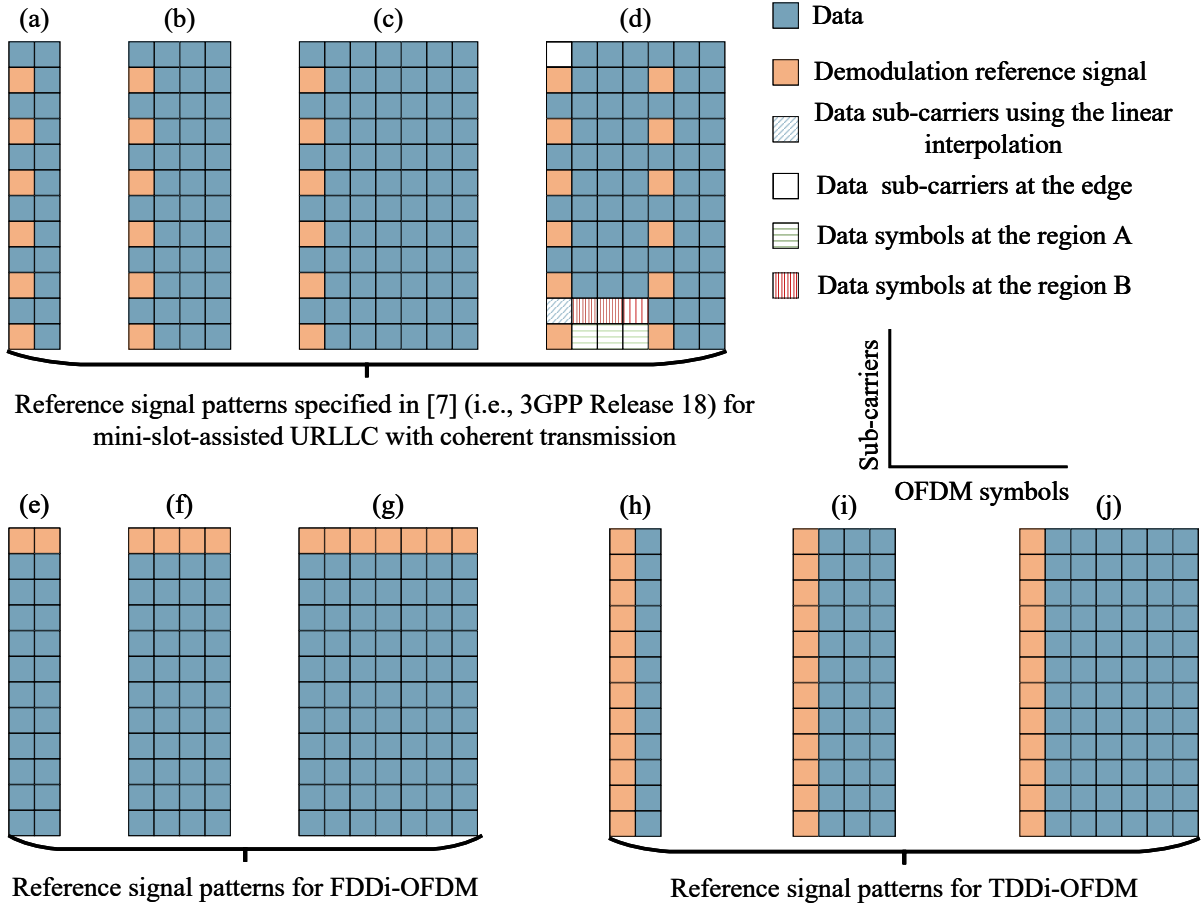


Fig. 1: Reference signal patterns of 2, 4 and 7 OFDM symbol units with coherent detection (a-d), frequency domain differential modulation (e-g), and time domain differential modulation (h-j). According to [7], the patterns (a) and (b) are used in both low and high mobility scenarios, (c) is used in low mobility scenarios, and (d) is used in high mobility scenarios.

desired data by directly comparing the phases between two successively received symbols, thereby eliminating the need for CSI (e.g. [12]–[14]). Furthermore, depending on whether DM is performed on adjacent subcarriers of the same OFDM symbol or on the same subcarrier of adjacent OFDM symbols, differential OFDM systems can be classified into frequency domain differential OFDM [15] and time domain differential OFDM [16]. These existing works on DM, however, are all aimed at conventional long packet/slot-based transmission. An interesting question is therefore how DM could be applied to SPT and how it would perform. For the former, based on the 3GPP mini-slot structures, DM can be implemented in the frequency domain, given the relatively small channel variation over two adjacent sub-carriers (especially for mmWave bands) - hence termed frequency domain differential OFDM (FDDi-OFDM) in this paper, as shown in Figs.1(e-g); or realized in the time domain, given the possibly small channel variation over two adjacent OFDM symbols - hence termed time domain differential OFDM (TDDi-OFDM) in this paper, as shown in Figs.1(h-j).

On the other hand, it is also worth noting that, in low mobility scenarios with 4 and 7 OFDM symbol units (as

illustrated in Fig.1), the DM scheme (especially the TDDi-OFDM scheme) still consumes a sizable (although less) reference signal overhead compared to the pilot-based coherent counterpart. This implies that, given the well known 3dB issue with DM, the pilot-based coherent detection scheme may still remain competitive in a slow fading environment when using a relatively medium or large sized mini-slot. Consequently, it may well be necessary to adaptively switch between differential and coherent modes based on application scenarios, channel statistics, information payloads, mini-slot deployment options and service requirements, minimizing the reference signal overhead and the impact on the reliability performance. Despite both non-coherent and coherent detection having in the past been investigated in wireless communications, the potential advantages of utilizing adaptively differential and coherent modulation modes for mini-slot-assisted short packet URLLC have not been explored in the literature, which constitutes the main motivation of this paper.

C. Related Works and Our Contributions

1) Pilot and coherent detection based SPT: Substantial research has delved into the performance of coherent detection

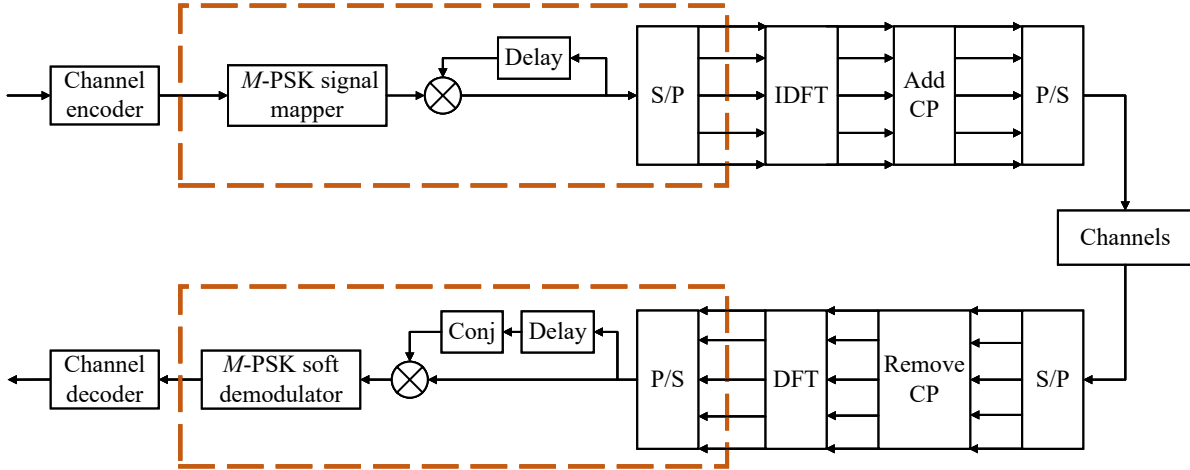


Fig. 2: Block diagram of FDDi-OFDM.

for short packet transmission (SPT) with perfect CSI over various types of channels, including ergodic fading channels [17], block fading channels [18] and quasi-static fading channels [19]. Building on these foundations, the impact of pilot lengths and mismatched CSI on the maximum achievable coded rate and packet error rate performance of SPT was studied for multiple antenna systems in [20], for massive multiple-input multiple-output (MIMO) systems in [21] and [22], and for cell-free massive MIMO systems in [23]. Additionally, there have been some attempts to optimize the channel estimation overhead for coherent SPT detection and URLLC. For example, in [24], the pilot length optimization of short packets considering the packet size and the error probability was investigated. In [25], joint optimization of pilot length and block length was explored for multi-device URLLC, developing dynamic and static optimization algorithms to maximize effective throughput with independent pilot or shared pilot frame structures. In [26], a partial superimposed pilot frame structure was introduced for SPT, proposing a joint pilot length, pilot power and payload power allocation algorithm to maximize the weighted sum rate of the presented scheme. Moreover, [27] investigated a data-assisted channel estimation approach to enhance the channel estimation quality with reduced training overheads in SPT. However, the non-asymptotic information theoretic results presented in [28] reveal that, for block-fading channels, non-coherent SPT is more energy efficient than its pilot-assisted counterpart with maximum likelihood (ML) channel estimation, even with pilot length and power optimized. Indeed, due to the inherent tradeoff between performance and signaling overhead under coherent SPT, optimizing the pilot length alone remains insufficient to minimize the reference signal overhead, particularly when the channel conditions change rapidly.

2) Non-coherent detection-based SPT: Given the high training cost in coherent detection schemes, research on non-coherent SPT detection has emerged as a topic of interest in URLLC. Specifically, in [29] and [30], the maximum achievable coded rate of non-coherent SPT detection over

single antenna Rayleigh block-fading channels was derived using normal approximation and saddlepoint methods, respectively. The results of non-coherent SPT detection under single antenna systems were subsequently extended to MIMO systems in [31]. Moreover, several studies have explored pilot-free designs for SPT in URLLC. For instance, in [32] and [33], a sparse vector coding approach without pilots was proposed for SPT where the decoding process relies on identifying nonzero elements of the received signals. However, this approach suffers from two main drawbacks: low spectral efficiency (especially when the sparse vector length is larger), and considerably diminished performance in high mobility scenarios. In [34], an iterative semi-blind receiver structure was proposed to enable mini-slot-assisted URLLC in short frame full duplex systems with carrier frequency offsets. In addition, in [35] and [36], a novel blind SPT strategy was introduced where the data is modulated onto the zero structure of the z -transform of the transmitted discrete-time baseband signal and the information is recovered by using either an ML detector or a simple direct zero-testing detector at the receiver. Unfortunately, the high computational complexity of the ML detector might render it unsuitable for URLLC. Conversely, while the direct zero-testing detector offers lower complexity, it experiences significant performance degradation, particularly in frequency-selective fading channels.

3) DM-based SPT: Surprisingly, DM has been largely overlooked in the literature related to URLLC except for [37] and [38]. In [37], a combination of DM and index modulation was proposed for OFDM-based pilot-free SPT, while in [38], differential preamble detection was applied to minimize the synchronization overhead of SPT. Despite these efforts, the theoretical analysis and comparative insight of DM based SPT have never been fully established. Our recent work [39] on single carrier systems has demonstrated, from an information theoretic perspective, that DM is a promising solution to achieve efficient SPT with low training overheads, providing helpful design insights for URLLC. Regrettably, although the aforementioned studies have considered the issue

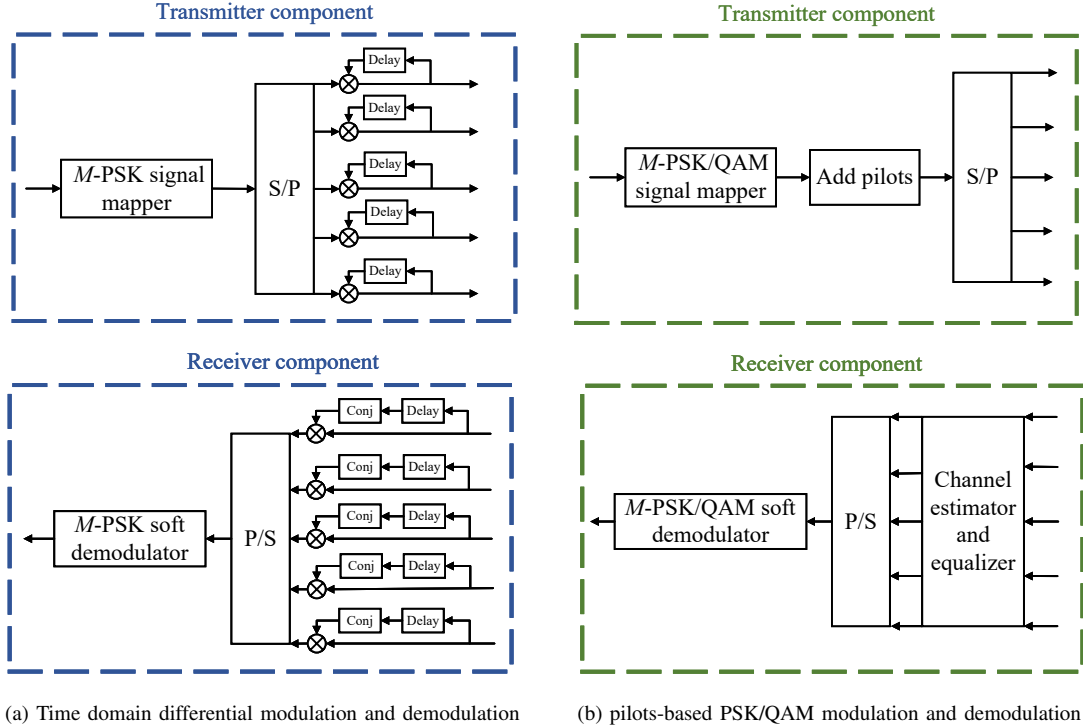


Fig. 3: Transceiver components of (a) TDDi-OFDM and (b) PA-OFDM.

of pilot overhead, the solutions are still imperfect in striking a balance among signaling overhead, system performance and computational complexity either by optimizing the pilot length [24]–[27] or by employing non-coherent detection [32]–[39]. Therefore, this paper aims to make a first step towards bridging this gap and tries to explore an efficient transmission paradigm based on adaptive non-coherent detection and coherent detection to achieve URLLC with an optimum reference signal overhead.

II. SYSTEM MODEL AND ASSUMPTIONS

In this paper, we consider a mini-slot-assisted single-input single-output URLLC system with K subcarriers and T consecutive OFDM symbols. We assume a bit sequence of emergency information $\mathbf{g} = \{g_1, g_2, \dots, g_B\}$ at the transmitter and B is the sequence length. In order to enhance the system reliability, a channel encoder is employed, transforming B information bits into a sequence of J coded bits. Furthermore, we consider an adaptive differential and pilot symbol-assisted OFDM transmission scheme to accommodate varying channel conditions and information payloads, minimizing the channel estimation overheads in short packet URLLC. Fig. 2 illustrates the block diagram of FDDi-OFDM. In addition, the transceiver components within the two dashed boxes of Fig. 2 can also be replaced with TDDi-OFDM [40] and conventional pilot symbol-assisted OFDM (PA-OFDM), as shown in Fig. 3. The details are as follows.

A. Differentially modulated OFDM

For differentially modulated OFDM, we first map the J coded bits into an M -ary phase-shift keying (M -PSK) symbol

block $\mathbf{c} = \{c_1, c_2, \dots, c_N\}$ of length $N = J/\log_2 M$, where $c_n \in \mathcal{X}^{\text{PSK}}$ and N is assumed to be an integer. Here, $\mathcal{X}^{\text{PSK}} = \{e^{j\varphi_m}\}_{m=0}^{M-1}$ is the constellation alphabet of M -PSK symbols and $\varphi_m = 2\pi m/M$ is the information-carrying phase. Moreover, depending on whether the differentially modulated symbols are placed on adjacent subcarriers within the same OFDM symbol duration or on the same subcarrier but across adjacent OFDM symbols, we can make a distinction between frequency domain and time domain differential OFDM. Specifically, we rearrange N -length PSK symbol block into a matrix $(v_{k,t})$ of size $(K-1) \times T$ for FDDi-OFDM. By contrast, in TDDi-OFDM, the N -length PSK symbol block is rearranged into a matrix $(v_{k,t})$ with dimensions $K \times (T-1)$. Then, the signal assigned to the k -th subcarrier of the t -th OFDM symbol, denoted as $d_{k,t}$, is given by [40, Eq.(15)]

$$d_{k,t} = \begin{cases} v_{k,t}d_{k-1,t}, & \text{FDDi-OFDM} \\ v_{k,t}d_{k,t-1}, & \text{TDDi-OFDM} \end{cases} \quad (1)$$

where $d_{0,t} = 1$ and $d_{k,0} = 1$ are the initial reference signal of the t -th OFDM symbol in FDDi-OFDM and of the k -th subcarrier in TDDi-OFDM, respectively.

In OFDM systems, the transmitted sequence is obtained by performing an K -point inverse discrete Fourier transform (IDFT) on $\{d_{k,t}\}_{k=0}^{K-1}$. Let L denote the maximum number of channel paths. A cyclic prefix (CP) of length L is then added in the transmitted sequence. Consequently, the transmitted sequence of the t -th OFDM symbol, including the CP, can

be expressed as

$$s_t(i) = \frac{1}{\sqrt{K}} \sum_{k=0}^{K-1} d_{k,t} e^{j2\pi ki/K}, \quad (2)$$

for $-L \leq i \leq K-1$. Moreover, the time-varying wide sense stationary uncorrelated scattering (WSSUS) Rayleigh fading channels with arbitrary power delay profiles are assumed, which can be modeled by tapped delay line models. In particular, we use $h_t(l)$ to denote the tap gain of the l -th path during the t -th OFDM symbol. For WSSUS Rayleigh fading channels, $h_t(l)$ of different channel paths is spatially uncorrelated and independent. We denote the normalized fading power of the l -th path as σ_l^2 . Then, we have $\sum_{l=1}^L \sigma_l^2 = 1$ and $h_t(l) \sim \mathcal{CN}(0, \sigma_l^2)$. Furthermore, Jakes' model is utilized to characterize the time-varying nature of the channels and the autocorrelation function of the l -th path is given by

$$\mathbb{E}\{h_{t+\Delta t}(l) h_t^*(l)\} = \sigma_l^2 \mathcal{J}_0(2\pi f_d T_s \Delta t), \quad (3)$$

where $\mathcal{J}_0(x)$ is the zero-th order Bessel function of the first kind, f_d is the Doppler frequency and T_s is the sampling period.

Based on $h_t(l)$, the channel frequency response at the k -th subcarrier of the t -th OFDM symbol can be written as

$$H_{k,t} = \sum_{l=0}^{L-1} h_t(l) e^{-j2\pi kl/K}. \quad (4)$$

Using (3) and (4), the time-frequency correlation function of $H_{k,t}$ for different symbols and subcarriers can be further expressed as

$$\begin{aligned} \rho(\Delta k, \Delta t) &= \mathbb{E}\{H_{k+\Delta k, t+\Delta t} H_{k,t}^*\} \\ &= \mathcal{J}_0(2\pi f_d T_s \Delta t) \sum_{l=0}^{L-1} \sigma_l^2 e^{-j2\pi l \Delta k/K}. \end{aligned} \quad (5)$$

It is worth noting that (5) reduces to

$$\rho_f(\Delta k) = \rho(\Delta k, 0) = \sum_{l=0}^{L-1} \sigma_l^2 e^{-j2\pi l \Delta k/K} \quad (6)$$

for $\Delta t = 0$ and

$$\rho_t(\Delta t) = \rho(0, \Delta t) = \mathcal{J}_0(2\pi f_d T_s \Delta t) \quad (7)$$

for $\Delta k = 0$. As a result, we can separate $\rho(\Delta k, \Delta t)$ as the product of the frequency domain correlation function $\rho_f(\Delta k)$ (depending on the multi-path delay profile) and the time domain correlation function $\rho_t(\Delta t)$ (depending on the mobility). Especially, the frequency domain correlation for two consecutive subcarriers of the same OFDM symbol is given by

$$\rho_f = \rho_f(1) = \sum_{l=0}^{L-1} \sigma_l^2 e^{-j2\pi l/K} \quad (8)$$

and the time domain correlation for two adjacent OFDM symbols on the same subcarrier is

$$\rho_t = \rho_t(1) = \mathcal{J}_0(2\pi f_d T_s) \quad (9)$$

With the assumption of perfect symbol synchronization, the

corresponding received signal of $s_t(i)$ after removing the CP is

$$r_t(i) = \sum_{l=0}^{L-1} h_t(l) s_t(i-l) + w_t(i), \quad (10)$$

for $0 \leq i \leq K-1$, where $w_t(i)$ represents the complex additive white Gaussian noise (AWGN) with zero mean and variance σ_w^2 . Then, computing a K -point discrete Fourier transform (DFT) of $\{r_t(i)\}_{i=0}^{K-1}$ yields the following expression for the received signal at the k -th subcarrier of the t -th OFDM symbol:

$$z_{k,t} = \frac{1}{\sqrt{K}} \sum_{i=0}^{K-1} r_t(i) e^{-j2\pi ki/K}. \quad (11)$$

Furthermore, by substituting (2) and (10) into (11), the received symbol after DFT can be rewritten as

$$\begin{aligned} z_{k,t} &= \underbrace{\left[\sum_{l=0}^{L-1} h_t(l) e^{-j2\pi kl/K} \right]}_{\text{Channel frequency response}} d_{k,t} + \underbrace{\frac{1}{\sqrt{K}} \sum_{i=0}^{K-1} w_t(i) e^{-j2\pi ki/K}}_{\text{Additive noise}} \\ &= H_{k,t} d_{k,t} + W_{k,t}. \end{aligned} \quad (12)$$

For the variance of $W_{k,t}$, we have

$$\mathbb{E}\{W_{k,t} W_{k,t}^*\} = \frac{1}{K} \sum_{i=0}^{K-1} \mathbb{E}\{w_t(i) w_t^*(i)\} = \sigma_w^2. \quad (13)$$

Therefore, the SNR for the transmitted signals in mini-slot-assisted OFDM is

$$\gamma = \frac{1}{\sigma_w^2}. \quad (14)$$

For differentially modulated OFDM, the information is detected at the receiver by comparing two received signals, which can be two adjacent signals on the same subcarrier, or two subcarrier signals during the same OFDM duration. Hence, the detected signal is given by

$$a_{k,t} = \begin{cases} z_{k,t} z_{k-1,t}^*, & \text{FDDi-OFDM} \\ z_{k,t} z_{k,t-1}^*, & \text{TDDi-OFDM} \end{cases} \quad (15)$$

Subsequently, the parallel detected signal is rearranged into a serial sequence and passed through the soft decision detector and the channel decoder. Finally, an estimate for the B -bit information, $\hat{\mathbf{g}} = \{\hat{g}_1, \hat{g}_2, \dots, \hat{g}_B\}$, is obtained at the receiver.

B. PA-OFDM

On the other hand, if coherent detection is used, the pilot symbols have to be inserted in mini-slot-assisted SPT to estimate CSI and detect information. The channel estimation performance, however, may heavily depend on the pilot patterns and the estimation schemes employed. For PA-OFDM, we employ the pilot patterns defined in 3GPP (i.e., [6] and [7]) for mini-slot-assisted URLLC. Specifically, let \mathcal{T} be the set of the pilot-carrying OFDM symbols. We assume that the pilot symbols are placed at equally spaced subcarriers of each OFDM symbol in \mathcal{T} , as shown in Figs. 1(a-d). Furthermore,

we denote the interval between pilot subcarriers as δ_{sub} and consider two widely used digital modulation schemes, namely PSK and QAM, in the system model for PA-OFDM. Then, the number of pilots for each pilot-carrying OFDM symbol is $\lambda_p = K/\delta_{sub}$ and the total number of the pilot symbols in the entire mini-slot-assisted OFDM is $\lambda_{total} = \lambda_p |\mathcal{T}|$.

At the receiver, we adopt a combination of LMMSE channel estimation and linear interpolation to obtain the estimated CSI of mini-slot-assisted OFDM. For the convenience of understanding, we divide resource elements in mini-slot-assisted OFDM into the following three distinct types.

- **Pilots:** Channel estimates at pilot subcarriers are computed using the LMMSE estimator. Let $\mathbf{H}_{t_p} = [H_{0,t_p} \ H_{\delta_{sub},t_p} \ \dots \ H_{(\lambda_p-1)\delta_{sub},t_p}]^T$ denote the channel responses at pilot subcarriers of a pilot-carrying OFDM symbol and $\hat{\mathbf{H}}_{\text{LMMSE}} = [\hat{H}_{0,t_p} \ \hat{H}_{\delta_{sub},t_p} \ \dots \ \hat{H}_{(\lambda_p-1)\delta_{sub},t_p}]^T$ denote the corresponding LMMSE estimates, where the index $t_p \in \mathcal{T}$. Then, the expression for $\hat{\mathbf{H}}_{\text{LMMSE}}$ is given by [41, Eq.(11)]

$$\hat{\mathbf{H}}_{\text{LMMSE}} = \mathbf{R}_{\mathbf{H}_{t_p}} \left(\mathbf{R}_{\mathbf{H}_{t_p}} + \frac{1}{\gamma} \mathbf{I} \right)^{-1} \hat{\mathbf{H}}_{\text{LS}} \quad (16)$$

where $\mathbf{R}_{\mathbf{H}_{t_p}} = \mathbb{E} \left\{ \mathbf{H}_{t_p} \mathbf{H}_{t_p}^H \right\}$ is the channel autocorrelation matrix at the pilot subcarriers, \mathbf{I} is the identity matrix and $\hat{\mathbf{H}}_{\text{LS}} = \begin{bmatrix} z_{0,t_p} & z_{\delta_{sub},t_p} & \dots & z_{(\lambda_p-1)\delta_{sub},t_p} \\ d_{0,t_p} & d_{\delta_{sub},t_p} & \dots & d_{(\lambda_p-1)\delta_{sub},t_p} \end{bmatrix}$ is the least-squares (LS) estimate of \mathbf{H}_{t_p} .

- **Data symbols within pilot-carrying OFDM symbols:** The linear interpolation technique is utilized to acquire CSI of data subcarriers lying between two pilot subcarriers. With the linear interpolation technique, the channel estimate of $(\lambda\delta_{sub} + k_d)$ -th data subcarriers is given by [42, Eq.(3)]

$$\hat{H}_{\lambda\delta_{sub}+k_d,t_p} = \frac{\delta_{sub} - k_d}{\delta_{sub}} \hat{H}_{\lambda\delta_{sub},t_p} + \frac{k_d}{\delta_{sub}} \hat{H}_{(\lambda+1)\delta_{sub},t_p} \quad (17)$$

for $\lambda = 0, \dots, \lambda_p - 2$ and $k_d = 1, \dots, \delta_{sub} - 1$. Note that the channel estimates for the data subcarriers that lie after the last pilot subcarrier cannot be obtained directly from (17). In such cases, we utilize the last and second-last pilot subcarriers to compute channel estimates for the data subcarriers at the edge, as expressed by [42, Eq.(4)]:

$$\begin{aligned} & \hat{H}_{(\lambda_p-1)\delta_{sub}+k_d,t_p} = \\ & - \frac{k_d}{\delta_{sub}} \hat{H}_{(\lambda_p-2)\delta_{sub},t_p} + \frac{\delta_{sub} + k_d}{\delta_{sub}} \hat{H}_{(\lambda_p-1)\delta_{sub},t_p} \end{aligned} \quad (18)$$

for $k_d = 1, \dots, \delta_{sub}$.

- **Data symbols that do not belong to pilot-carrying OFDM symbols:** The channel estimates for data symbols that do not belong to pilot-carrying OFDM symbols are assumed to be a reuse of the channel estimates from pilot-carrying OFDM symbols. Specifically, data symbols that do not belong to pilot-carrying OFDM symbols can be further divided into two types: data symbols at the region A and B, as illustrated in Fig.1(d). In Region A, the estimated CSI of the pilot sub-carriers is directly used to detect data

symbols while in Region B, the channel estimates of data symbols are obtained by directly utilizing the estimated CSI of data sub-carriers using the linear interpolation.

Based on the estimated CSI, we can detect the transmitted information for PA-OFDM.

III. PERFORMANCE ANALYSIS OF MINI-SLOT-ASSISTED SHORT PACKET OFDM

A. Preliminaries on Non-Asymptotic Information Theory

In information theory, a well-established result is that any reliable communications can be achieved with an infinite blocklength as long as the transmission rate remains below the channel capacity. Consequently, the classical Shannon's capacity formula serves as a performance metric for designing communication systems with an asymptotically large blocklength. However, such a canonical principle is unsuitable for the performance analysis and system design of SPT in URLLC due to the inherently constrained blocklength. To address this limitation in SPT, Polyanskiy et al. in [43] developed several non-asymptotic upper and lower bounds on the maximum coded rate and the smallest error probability. Here, we briefly review a specific pair of upper and lower bounds on the smallest error probability introduced in [43], commonly referred to as the information spectrum (IS) and dependence testing (DT) bounds, which play a crucial role in our subsequent analysis. For the convenience of our derivation next, the IS and DT bounds, as derived in [43], are included below.

Theorem 1 (*IS lower bound [43, Th.11]*): For a general P2P channel consists of an input alphabet \mathcal{X} , an output alphabet \mathcal{Y} and a conditional channel transition probability $\mathbb{P}_{Y^{\bar{N}}|X^{\bar{N}}}(y^{\bar{N}}|x^{\bar{N}}) : \mathcal{X}^{\bar{N}} \rightarrow \mathcal{Y}^{\bar{N}}$ with blocklength \bar{N} , the minimum achievable BLER ε with information bits of length B is lower-bounded as

$$\varepsilon \geq \sup_{\beta > 0} \left\{ \inf_{\mathbb{P}_X} \mathbb{P} \left[i(X^{\bar{N}}; Y^{\bar{N}}) \leq \log_2 \beta \right] - \frac{\beta}{2B} \right\} \quad (19)$$

where $\beta > 0$ is an arbitrary positive constant and

$$i(X^{\bar{N}}; Y^{\bar{N}}) = \log_2 \frac{\mathbb{P}_{Y^{\bar{N}}|X^{\bar{N}}}(y^{\bar{N}}|x^{\bar{N}})}{\mathbb{P}_{Y^{\bar{N}}}(y^{\bar{N}})} \quad (20)$$

is termed the information density.

Theorem 2 (*DT upper bound [43, Th.17]*): For a general P2P channel $\mathbb{P}_{Y^{\bar{N}}|X^{\bar{N}}}(y^{\bar{N}}|x^{\bar{N}})$, the minimum achievable BLER ε with information bits of length B is upper-bounded as

$$\varepsilon \leq \mathbb{E} \left[\exp \left\{ - \left[i(X^{\bar{N}}; Y^{\bar{N}}) - \log_2 \left((2^B - 1) / 2 \right) \right]^+ \right\} \right], \quad (21)$$

where $[A]^+ = A$ if $A \geq 0$ and 0 otherwise.

Obviously, the IS lower bound signifies an impossible result: for a given blocklength, encoding and decoding schemes that lie below the IS bound are unattainable. Conversely, the upper bound indicates there exist some encoding and decoding schemes whose performance is at least as good as the DT bound, despite the method of constructing such

these schemes being unknown. Note that the non-asymptotic bounds presented in [43] are applicable for SPT under any P2P channels, enabling us to utilize the IS and DT bounds to evaluate the error probability of mini-slot-assisted short packet URLLC. Moreover, to describe the asymptotic behavior of the non-asymptotic upper and lower bounds, [43] derived an elegant approximation formula for the maximum coded rate and the minimum error probability under P2P Gaussian channels. In particular, the maximum achievable rate (bits/symbol, bits/s/Hz or bits/channel use) for P2P Gaussian channels can be tightly approximated as the following function of blocklength \bar{N} , error probability ε and SNR γ [43, Eq.(296)]:

$$R \approx C(\gamma) - \sqrt{\frac{V(\gamma)}{\bar{N}}} Q^{-1}(\varepsilon) + \frac{\log_2 \bar{N}}{2\bar{N}}. \quad (22)$$

Here $C(\gamma) = \log_2(1 + \gamma)$ is the complex AWGN channel capacity, $V(\gamma) = \gamma(2 + \gamma)/(1 + \gamma)^2$ is known as channel dispersion and $Q^{-1}(\cdot)$ is the inverse of the Gaussian Q-function. Furthermore, for a fixed rate $R = B/\bar{N}$ and blocklength, the minimum achievable BLER under P2P Gaussian channels can be equivalently expressed as [9, Eq.(23)]

$$\varepsilon \approx Q \left(\sqrt{\frac{\bar{N}}{V(\gamma)}} \left(C(\gamma) - R + \frac{\log_2 \bar{N}}{2\bar{N}} \right) \right). \quad (23)$$

The expression (22) and (23), which are usually termed normal approximation, rely on a central-limit-theorem analysis and characterize the interplay among the rate, reliability and blocklength in SPT under AWGN channels. Building on this seminal contribution, subsequent studies (e.g. [17]–[23], [28]–[31] and [44]–[46]) have generalized the achievable rate and the minimum achievable BLER formula under AWGN to various channels and communication models by employing the non-asymptotic information-theoretic bounds and normal approximation results proposed in [43]. However, it is worth noting that most existing SPT performance results are based on the assumption of continuous Gaussian signals as channel inputs, except [47] which presented the maximum achievable rate for AWGN channels with QAM or PSK inputs. Nevertheless, extending these SPT performance results to mini-slot-assisted OFDM systems with discrete inputs is still challenging due to imperfect CSI, frequency selective and temporally correlated channels.

B. Differentially Modulated Short Packet OFDM

Based on the aforementioned non-asymptotic information-theoretic bounds, we can derive the performance of differentially modulated short packet OFDM. Let N_{dif} denote the number of available data symbols in differential OFDM. Thus, we have $N_{\text{dif}} = (K - 1)T$ for FDDi-OFDM and $N_{\text{dif}} = K(T - 1)$ for TDDi-OFDM. Additionally, we use $I_{\text{dif}}(\gamma)$ and $V_{\text{dif}}(\gamma)$ to denote the expectation and variance of

the information density for differential OFDM with a single channel use, respectively. Specifically, $I_{\text{dif}}(\gamma)$ and $V_{\text{dif}}(\gamma)$ for FDDi-OFDM are given in (42) and (43) in Appendix A. Similarly, $I_{\text{dif}}(\gamma)$ and $V_{\text{dif}}(\gamma)$ for TDDi-OFDM can be obtained using the same procedures with the variable ρ_f in (42) and (43) replaced by ρ_t . Here, ρ_t is the time domain correlation defined in (9). Then, the performance of differentially modulated short packet OFDM can be described in the following theorem:

Theorem 3 (*Differentially modulated OFDM*): For both frequency and time domain differential OFDM, the maximum achievable rate can be determined as

$$R \approx I_{\text{dif}}(\gamma) - \sqrt{\frac{V_{\text{dif}}(\gamma)}{N_{\text{dif}}}} Q^{-1}(\varepsilon) + \frac{\log_2 N_{\text{dif}}}{2N_{\text{dif}}}. \quad (24)$$

The minimum achievable BLER of differentially modulated OFDM for given rate R can be approximately expressed as

$$\varepsilon \approx Q \left(\sqrt{\frac{N_{\text{dif}}}{V_{\text{dif}}(\gamma)}} \left(I_{\text{dif}}(\gamma) - R + \frac{\log_2 N_{\text{dif}}}{2N_{\text{dif}}} \right) \right). \quad (25)$$

Proof: See Appendix A. ■

We note that the results in Theorem 3 are similar to the normal approximation given by (22) and (23) for the optimal continuous input AWGN channel, with capacity and dispersion replaced by $I_{\text{dif}}(\gamma)$ and $V_{\text{dif}}(\gamma)$. Therefore, $I_{\text{dif}}(\gamma)$ and $V_{\text{dif}}(\gamma)$ can be respectively regarded as the channel capacity and dispersion for differentially modulated OFDM.

C. Pilot Symbol-assisted Short Packet OFDM

In this subsection, the performance of pilot symbol-based short packet OFDM is analysed. Specifically, the average channel estimation MSE is first evaluated for the pilot patterns and estimation schemes considered in Section II-B, which helps in quantifying the SNR penalty due to imperfect channel estimation in PA-OFDM. Then, based on the average channel estimation MSE and the effective SNR, we can derive closed-form expressions (i.e., normal approximation) for the performance of pilot symbol-based short packet OFDM with imperfect channel estimation.

Let $\hat{H}_{k,t} = H_{k,t} - e_{k,t}$ denote the channel estimate of $H_{k,t}$, where $e_{k,t}$ is the corresponding channel estimation error. Then, for PA-OFDM, the expression in (12) can be rewritten as

$$z_{k,t} = \hat{H}_{k,t} d_{k,t} + e_{k,t} d_{k,t} + W_{k,t}. \quad (26)$$

For simplicity, we use σ_e^2 to represent the variance of $e_{k,t}$ and assume that $e_{k,t}$ and $H_{k,t}$ are statistically independent. From (26), the effective SNR for PA-OFDM becomes

$$\hat{\gamma} = \frac{1 - \sigma_e^2}{\sigma_e^2 + \sigma_w^2}. \quad (27)$$

According to the channel estimation scheme in Section II-B and the pilot pattern in Fig.1, σ_e^2 is mainly determined by the

$$\sigma_e^2 = \frac{\lambda_p}{K\delta_{sym}} \Phi_{\text{LMMSE}} + \left(\frac{K - \lambda_p}{K\delta_{sym}} - \frac{\delta_{sub} - 1}{K\delta_{sym}} \right) \Phi_{\text{linear}} + \frac{\delta_{sub} - 1}{K\delta_{sym}} \Phi_{\text{edge}} + \frac{\lambda_p (\delta_{sym} - 1)}{K\delta_{sym}} \Phi_{\text{A}} + \frac{(K - \lambda_p) (\delta_{sym} - 1)}{K\delta_{sym}} \Phi_{\text{B}} \quad (28)$$

channel estimation error on pilot subcarriers, data subcarriers using the linear interpolation, data subcarriers at the edge and data symbols at the regions A and B. Thus, to characterize the SNR penalty due to the channel estimation error at these resource elements, we use the average channel estimation MSE to evaluate σ_e^2 , as in [48] and [49]. In particular, the average channel estimation MSE can be expressed as a weighted mean of the MSE of the different resource element types. We represent the interval between two adjacent pilot-carrying OFDM symbols in \mathcal{T} as δ_{sym} . Especially, if there is only one pilot-carrying OFDM symbol in mini-slot (i.e., $|\mathcal{T}| = 1$), the symbol interval is $\delta_{sym} = T$. Then, for the resource elements at the OFDM symbol interval δ_{sym} , the average channel estimation MSE is given by (28), where Φ_{LMMSE} , Φ_{linear} , Φ_{edge} , Φ_A and Φ_B are respectively the channel estimation MSE for pilot subcarriers, data subcarriers using the linear interpolation, data subcarriers at the edge and data symbols at regions A and B. Since the number of the data subcarriers at the edge is very small in mini-slot-assisted OFDM, we ignore the difference between Φ_{linear} and Φ_{edge} for simplicity. Therefore, (28) can be simplified as

$$\begin{aligned} \sigma_e^2 &= \frac{\lambda_p \Phi_{\text{LMMSE}}}{K \delta_{sym}} + \frac{(K - \lambda_p) \Phi_{\text{linear}}}{K \delta_{sym}} + \frac{\lambda_p (\delta_{sym} - 1)}{K \delta_{sym}} \Phi_A \\ &+ \frac{(K - \lambda_p) (\delta_{sym} - 1)}{K \delta_{sym}} \Phi_B. \end{aligned} \quad (29)$$

For the LMMSE channel estimator in (16), the MSE Φ_{LMMSE} is given by [50]

$$\begin{aligned} \Phi_{\text{LMMSE}} &= \frac{1}{\lambda_p} \sum_{\lambda=0}^{\lambda_p-1} \mathbb{E} \left\{ \left\| \widehat{H}_{\lambda \delta_{sub}, t_p} - H_{\lambda \delta_{sub}, t_p} \right\|^2 \right\} \\ &= \frac{1}{\lambda_p} \text{tr} \left(\mathbf{R}_{\mathbf{H}_{t_p}} \left(\mathbf{I} - \left(\mathbf{R}_{\mathbf{H}_{t_p}} + \frac{\mathbf{I}}{\gamma} \right)^{-1} \mathbf{R}_{\mathbf{H}_{t_p}} \right) \right) \\ &= \frac{1}{\lambda_p} \sum_{\lambda=0}^{\lambda_p-1} \frac{\psi_\lambda}{\gamma \psi_\lambda + 1}, \end{aligned} \quad (29)$$

where $\{\psi_\lambda\}_{\lambda=0}^{\lambda_p-1}$ are the eigenvalues of $\mathbf{R}_{\mathbf{H}_{t_p}}$. In addition, the MSE Φ_{linear} can be derived as in (30), where (a) follows from

(17) and the fact that $\mathbb{E} \left\{ \left\| a H_{\lambda \delta_{sub}, t_p} + b H_{(\lambda+1) \delta_{sub}, t_p} \right\|^2 \right\} = \mathbb{E} \left\{ \left\| a H_{\lambda \delta_{sub}, t_p} \right\|^2 \right\} + 2 \Re \left\{ \mathbb{E} \left\{ a b H_{\lambda \delta_{sub}, t_p}^* H_{(\lambda+1) \delta_{sub}, t_p} \right\} \right\} + \mathbb{E} \left\{ \left\| b H_{(\lambda+1) \delta_{sub}, t_p} \right\|^2 \right\}$ for any constants a and b , while (b) is due to the result of (5) and $\mathcal{L} = \frac{5\delta_{sub}-1}{3\delta_{sub}} + \frac{\delta_{sub}+1}{3\delta_{sub}} \Re(\rho(\delta_{sub}, 0)) + \frac{2\delta_{sub}-1}{3\delta_{sub}} \Phi_{\text{LMMSE}}$. Similarly to the derivation in (30), Φ_A and Φ_B can be respectively expressed as

$$\begin{aligned} \Phi_A &= \frac{1}{\lambda_p (\delta_{sym} - 1)} \\ &\times \sum_{\delta=1}^{\delta_{sym}-1} \sum_{\lambda=0}^{\lambda_p-1} \mathbb{E} \left\{ \left\| \widehat{H}_{\lambda \delta_{sub}, t_p} - H_{\lambda \delta_{sub}, t_p + \delta} \right\|^2 \right\} \\ &= 2 + \Phi_{\text{LMMSE}} - \frac{2}{\delta_{sym} - 1} \sum_{\delta=1}^{\delta_{sym}-1} \rho(0, \delta), \end{aligned} \quad (31)$$

and

$$\begin{aligned} \Phi_B &= \frac{1}{(\lambda_p - 1) (\delta_{sym} - 1) (\delta_{sub} - 1)} \times \\ &\sum_{\delta=1}^{\delta_{sym}-1} \sum_{k_d=1}^{\delta_{sub}-1} \sum_{\lambda=0}^{\lambda_p-1} \mathbb{E} \left\{ \left\| \widehat{H}_{\lambda \delta_{sub} + k_d, t_p} - H_{\lambda \delta_{sub} + k_d, t_p + \delta} \right\|^2 \right\} \\ &= \mathcal{L} - \frac{2}{(\delta_{sym} - 1) (\delta_{sub} - 1)} \sum_{\delta=1}^{\delta_{sym}-1} \sum_{k_d=1}^{\delta_{sub}-1} \left[\frac{\delta_{sub} - k_d}{\delta_{sub}} \right. \\ &\times \left. \Re(\rho(k_d, \delta)) + \frac{k_d}{\delta_{sub}} \Re(\rho(k_d - \delta_{sub}, \delta)) \right]. \end{aligned} \quad (32)$$

Finally, combining (27) and (29)-(32) leads to the effective SNR $\widehat{\gamma}$ for PA-OFDM.

Note that the single carrier SPT performance of ergodic fading channels with independent and identically distributed (i.i.d) PSK/QAM channel inputs and perfect CSI has been analysed in [39]. Similarly, the performance results derived in [39] for coherent fading channels with i.i.d PSK/QAM channel inputs are basically analogous to the normal approximation (22) and (23), with $I(\gamma)$ and $V(\gamma)$ replaced by the channel capacity and dispersion of i.i.d PSK/QAM inputs. To be specific, the coherent channel capacity with i.i.d PSK/QAM

$$\begin{aligned} \Phi_{\text{linear}} &= \frac{1}{\delta_{sub} - 1} \sum_{k_d=1}^{\delta_{sub}-1} \frac{1}{\lambda_p - 1} \sum_{\lambda=0}^{\lambda_p-2} \mathbb{E} \left\{ \left\| \widehat{H}_{\lambda \delta_{sub} + k_d, t_p} - H_{\lambda \delta_{sub} + k_d, t_p} \right\|^2 \right\} \\ &\stackrel{(a)}{=} \frac{1}{\delta_{sub} - 1} \sum_{k_d=1}^{\delta_{sub}-1} \frac{1}{\lambda_p - 1} \sum_{\lambda=0}^{\lambda_p-2} \mathbb{E} \left\{ H_{\lambda \delta_{sub} + k_d, t_p}^2 \right\} + \mathbb{E} \left\{ \left\| \frac{\delta_{sub} - k_d}{\delta_{sub}} H_{\lambda \delta_{sub}, t_p} \right\|^2 \right\} + \mathbb{E} \left\{ \left\| \frac{k_d}{\delta_{sub}} H_{(\lambda+1) \delta_{sub}, t_p} \right\|^2 \right\} \\ &+ 2 \Re \left\{ \mathbb{E} \left\{ \frac{(\delta_{sub} - k_d) k_d}{\delta_{sub}^2} H_{\lambda \delta_{sub}, t_p}^* H_{(\lambda+1) \delta_{sub}, t_p} \right\} \right\} + \mathbb{E} \left\{ \left\| \frac{\delta_{sub} - k_d}{\delta_{sub}} e^{\lambda \delta_{sub}, t_p} + \frac{k_d}{\delta_{sub}} e^{(\lambda+1) \delta_{sub}, t_p} \right\|^2 \right\} \\ &- 2 \Re \left\{ \mathbb{E} \left\{ H_{\lambda \delta_{sub} + k_d, t_p}^* \left(\frac{\delta_{sub} - k_d}{\delta_{sub}} H_{\lambda \delta_{sub}, t_p} + \frac{k_d}{\delta_{sub}} H_{(\lambda+1) \delta_{sub}, t_p} \right) \right\} \right\} \\ &\stackrel{(b)}{=} \mathcal{L} - \frac{2}{\delta_{sub} - 1} \sum_{k_d=1}^{\delta_{sub}-1} \left[\frac{\delta_{sub} - k_d}{\delta_{sub}} \Re(\rho(k_d, 0)) + \frac{k_d}{\delta_{sub}} \Re(\rho(k_d - \delta_{sub}, 0)) \right] \end{aligned} \quad (30)$$

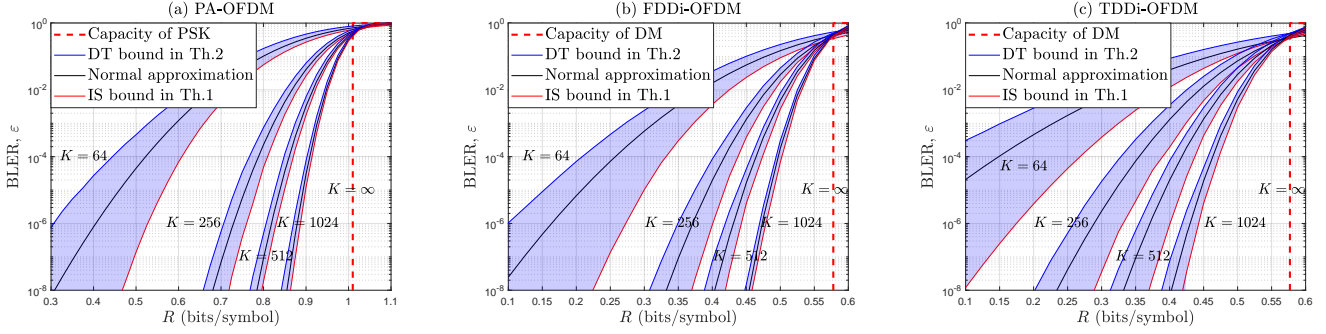


Fig. 4: The BLER performance of PA-OFDM, FDDi-OFDM and TDDi-OFDM for different K under a 2 OFDM symbol unit with modulation order $M = 4$, $f_d T_s = 0.01$, $L = 5$ and SNR $\gamma = 2$ dB.

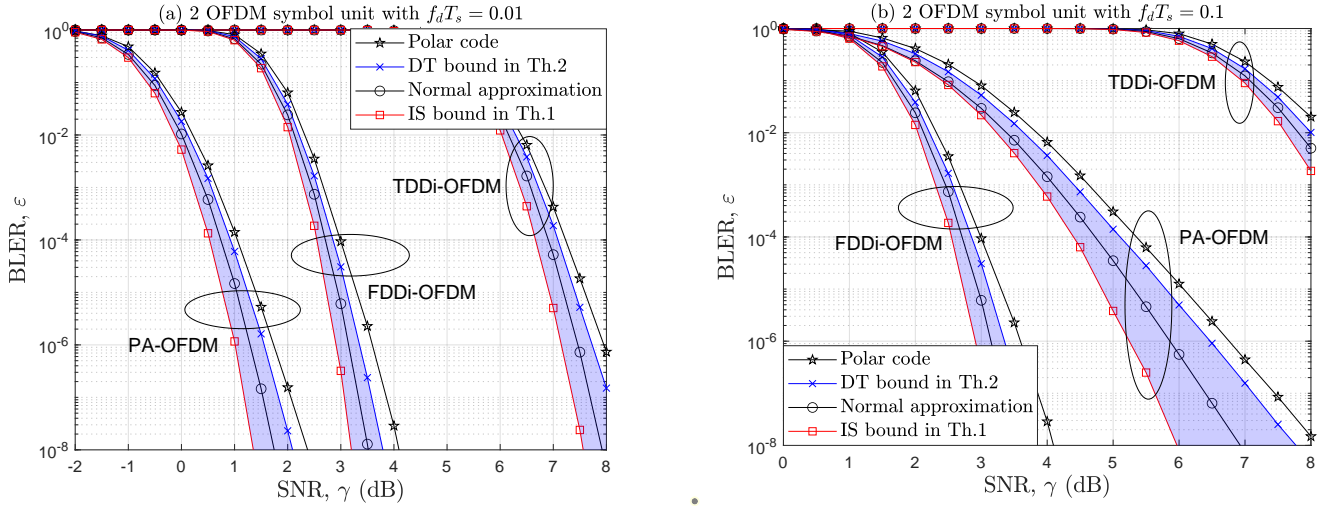


Fig. 5: BLER performance comparisons of PA-OFDM, FDDi-OFDM and TDDi-OFDM under a 2 OFDM symbol unit: (a) $f_d T_s = 0.01$, and (b) $f_d T_s = 0.1$.

inputs is given by [39, Eq.(15)]

$$I_{\text{coh}}(\gamma) = \log_2 M - \frac{1}{M} \sum_{j=1}^M \mathbb{E} \left[\log_2 \sum_{i=1}^M \exp \left(w^2 - (w + \sqrt{\gamma} h(x_j - x_i))^2 \right) \right] \quad (33)$$

and the coherent channel dispersion with i.i.d PSK/QAM inputs can be written as [39, Eq.(16)]

$$V_{\text{coh}}(\gamma) = -(\log_2 M - I_{\text{coh}}(\gamma))^2 + \frac{1}{M} \times \sum_{j=1}^M \mathbb{E} \left[\left\{ \log_2 \sum_{i=1}^M \exp \left(w^2 - (w + \sqrt{\gamma} h(x_j - x_i))^2 \right) \right\}^2 \right] \quad (34)$$

where $w \sim \mathcal{CN}(0, 1)$ is the unit-power noise component, the variables x_i and $x_j \in \mathcal{X}^{\text{PSK}}$ for PSK inputs and the variables x_i and $x_j \in \mathcal{X}^{\text{QAM}}$ for QAM inputs. Here, $\mathcal{X}^{\text{QAM}} = \sqrt{\frac{1}{\xi}} \times \{\pm(2m-1) \pm (2m-1)j\}$ is the input alphabet of an M -ary QAM constellation, where $m \in \{1, \dots, \frac{\sqrt{M}}{2}\}$ and $\xi = \frac{2(M-1)}{3}$ is a constant to normalize the average transmit power to unity. Then, based on the results in [39] and the effective SNR for

PA-OFDM, we have the following corollary:

Corollary 1 (*Pilot symbol-assisted short packet OFDM*): For the pilot patterns and the channel estimation schemes considered in Section II-B, the maximum achievable rate with PSK/QAM inputs can be written as

$$R \approx I_{\text{coh}}(\hat{\gamma}) - \sqrt{\frac{V_{\text{coh}}(\hat{\gamma})}{N_{\text{coh}}}} Q^{-1}(\varepsilon) + \frac{\log_2 N_{\text{coh}}}{2N_{\text{coh}}}, \quad (35)$$

where $N_{\text{coh}} = KT - \lambda_{\text{total}}$ is the number of available data symbols in PA-OFDM. The minimum achievable BLER can be approximately determined as

$$\varepsilon \approx Q \left(\sqrt{\frac{N_{\text{coh}}}{V_{\text{coh}}(\hat{\gamma})}} \left(I_{\text{coh}}(\hat{\gamma}) - R + \frac{\log_2 N_{\text{coh}}}{2N_{\text{coh}}} \right) \right). \quad (36)$$

IV. SIMULATION RESULTS

In this section, we compare the analytical BLER performance (i.e., normal approximation) of PA-OFDM, FDDi-OFDM and TDDi-OFDM. Furthermore, we employ Monte Carlo simulations to obtain the simulated BLER results and verify the correctness of our analysis. To be specific, for each

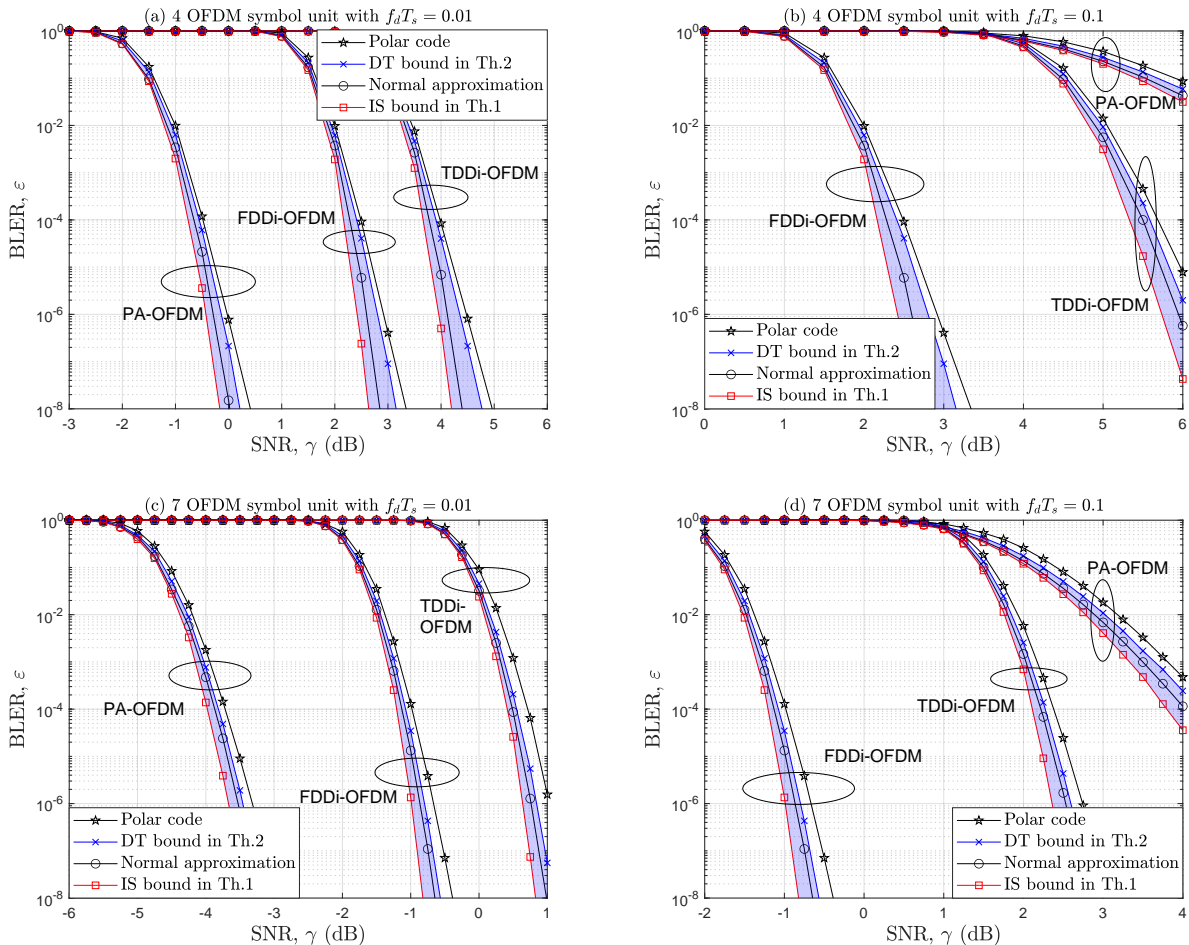


Fig. 6: BLER performance comparisons of PA-OFDM, FDDi-OFDM and TDDi-OFDM under a 4 or 7 OFDM symbol unit.

SNR value, we utilize 10^9 packet samples to compute the IS bound in Theorem 1 and the DT bound in Theorem 2. On the other hand, since the non-asymptotic bounds developed in [43] are based on optimal encoder-decoder pairs, there may be a gap between the normal approximation results and the performance achievable by actual coding schemes. To show how close actual encoder-decoder pairs perform to the normal approximation results derived in this paper, we employ cyclic redundancy check (CRC)-aided polar encoding and successive cancellation list (SCL) decoding schemes, as in [51]. Specifically, a 6-bit CRC code with the generator polynomial $x^6 + x^5 + 1$ is appended to B information bits. The CRC-appended information bits are then polar-encoded and rate-matched to output J information bits, forming a (J, B) polar encoder. For decoding, we use an SCL algorithm with a list size of 32 to generate the estimated information bits. In the polar coding-based Monte Carlo simulations, the simulated BLER for each SNR value is calculated after 100 packet errors have been observed. In addition, we adopt an exponentially decaying power-delay profile for the multi-path channel.

Fig.4 illustrates the BLER performance of PA-OFDM, FDDi-OFDM and TDDi-OFDM for different numbers of sub-carriers K (also means different values of the blocklength)

under a 2 OFDM symbol unit. Especially, the pilot pattern in Fig.1(a) is adopted for PA-OFDM (i.e., the set of the pilot-carrying OFDM symbols $\mathcal{T} = \{1\}$ and the interval between pilot sub-carriers $\delta_{sub} = 2$). In the figure, the SNR value is set to be $\gamma = 2$ dB and the dashed vertical red line denotes the corresponding channel capacity result. As shown in Fig.4, the normal approximation, IS bound and DT bound-based BLER results gradually approach the dashed vertical red line with the increase of K (also blocklength). Moreover, it is evident that the normal approximation results for PA-OFDM, FDDi-OFDM and TDDi-OFDM lie within a specific region (highlighted in blue) bounded by their respective IS and DT bounds. Therefore, the normal approximation results proposed in this paper provide satisfactory accuracy and low computational complexity in characterizing the minimum achievable BLER performance of PA-OFDM, FDDi-OFDM and TDDi-OFDM.

Figs.5-7 provide a BLER performance comparison of pilot-based, frequency domain differential and time domain differential OFDM under different normalized Doppler values, mini-slot deployment options and modulation orders. Notably, PA-OFDM suffers from a capacity and energy loss compared to differentially modulated OFDM due to the use of pilot symbols. Therefore, to ensure a fair comparison, it is essential to make the net data rates and power (or energy per block)

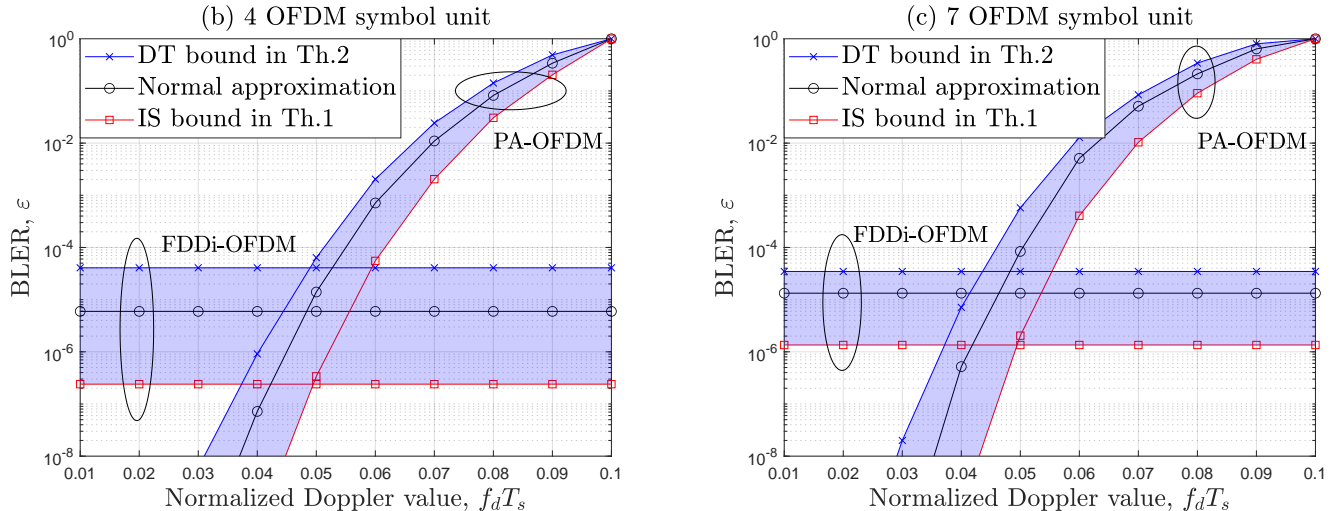


Fig. 7: BLER comparisons of PA-OFDM and FDDi-OFDM for different normalized Doppler values: (a) 4 OFDM symbol unit with $\gamma = 2.5$ dB and (b) 7 OFDM symbol unit with $\gamma = -1$ dB.

of PA-OFDM, FDDi-OFDM, and TDDi-OFDM consistent. In general, there are two design approaches for the pilot-assisted scheme and DM to achieve the same data rate and power. One approach is to adopt different modulation orders for the pilot-assisted scheme and DM, as utilized in [39]. Another easier approach is to use different coding rate for the pilot-assisted scheme and DM. For example, if BPSK and a code of rate $\frac{1}{5}$ are used in the pilot-assisted scheme to transmit 100 information bits and the number of pilots for the channel estimation is assumed to be 100 bits, the transmitting blocklength is thus 600 bits. For DM, a channel code of rate $\frac{1}{6}$ can be utilized to obtain the same transmit blocklength, achieving the same data rate as the pilot-assisted scheme. In our simulation result, the second approaches is employed to design PA-OFDM, FDDi-OFDM and TDDi-OFDM.

In Fig.5, the BLER performance of PA-OFDM, FDDi-OFDM and TDDi-OFDM with a 2 OFDM symbol unit is illustrated under normalized Doppler value $f_d T_s = 0.01, 0.1$. Specifically, the order of modulation is $M = 4$ and the numbers of the paths, sub-carriers and information bits are $L = 5$, $K = 256$ and $B = 256$, respectively. Additionally, for PA-OFDM, the set of the pilot-carrying OFDM symbols is $\mathcal{T} = \{1\}$ (i.e., pilots are placed at the first OFDM symbol of the mini-slot) and the interval between pilot sub-carriers is $\delta_{sub} = 2$ (corresponds to the pilot pattern in Fig.1(a)). Consequently, the available number of data symbol is $N_{coh} = 384$ for PA-OFDM, $N_{dif} = 510$ for FDDi-OFDM and $N_{dif} = 256$ for TDDi-OFDM. Moreover, the coding rate is $\frac{256}{384 \times 2}$ for PA-OFDM, $\frac{256}{510 \times 2}$ for FDDi-OFDM and $\frac{256}{256 \times 2}$ for TDDi-OFDM. From Fig.4(a), PA-OFDM shows a significant advantage over frequency domain and time domain differential OFDM in terms of the normal approximation, IS bound, DT bound and polar coding-based BLER results. Moreover, we note that PA-OFDM achieves an approximately 1-3 dB performance advantage compared with FDDi-OFDM for a low normalized Doppler value. However, the BLER performance of FDDi-OFDM surpasses that of PA-OFDM for

a high normalized Doppler value, as shown in Fig. 5(b). This advantage arises from two primary factors: (1) The detection of FDDi-OFDM mainly relies on the received symbols of two adjacent sub-carriers, making it robust against time-selective fading channels. (2) Unlike PA-OFDM, FDDi-OFDM does not incur the costly pilot overhead in SPT. Consequently, the saved bandwidth, power, and signal overhead can be utilized to generate a stronger channel code (i.e., a lower coding rate), improving the system reliability performance.

Fig.6 shows that the BLER performance of PA-OFDM, FDDi-OFDM and TDDi-OFDM with a 4 or 7 OFDM symbol unit. The system parameters for Fig.5 are: $L = 5$, $K = 256$, $\delta_{sub} = 2$ and the number of the information bits $B = 512$. In addition, 8-ary PSK and 16-ary QAM are adopted in PA-OFDM for 4 OFDM symbol units and 7 OFDM symbol units, respectively. Similarly, the modulation order of FDDi-OFDM and TDDi-OFDM is set to be $M = 8$ for a 4 OFDM symbol unit and $M = 16$ for a 7 OFDM symbol unit. Especially, for 7 OFDM symbol units with $f_d T_s = 0.1$, the set of the pilot-carrying OFDM symbols is $\mathcal{T} = \{1, 5\}$ (i.e., pilots are placed at the first and 5-th OFDM symbol of the mini-slot, which corresponds to the pilot pattern in Fig.1(d)). By contrast, the set of the pilot-carrying OFDM symbols for Fig.6(a-c) is $\mathcal{T} = \{1\}$ (corresponds to the pilot pattern in Fig.1(b) and Fig.1(c)). From Fig.6, the normal approximation, IS bound, DT bound and polar coding-based results show that the BLER performance of PA-OFDM outperforms that of FDDi-OFDM and TDDi-OFDM in a low Doppler environment for both 4 or 7 OFDM symbol units. Instead, for a high Doppler environment (e.g., $f_d T_s = 0.1$ in Fig.6(b) and Fig.6(d)), PA-OFDM has yielded the worst results. This is because, compared to the 2 OFDM symbol unit in Fig.1(a), PA-OFDM of 4 or 7 symbol units in Fig.1(b-d) introduce more data symbol (i.e., decreases the pilot percentage) and thus far more sensitive to channel variation.

Fig.7 illustrates a comparison of the BLER performance for PA-OFDM and FDDi-OFDM under different normalized

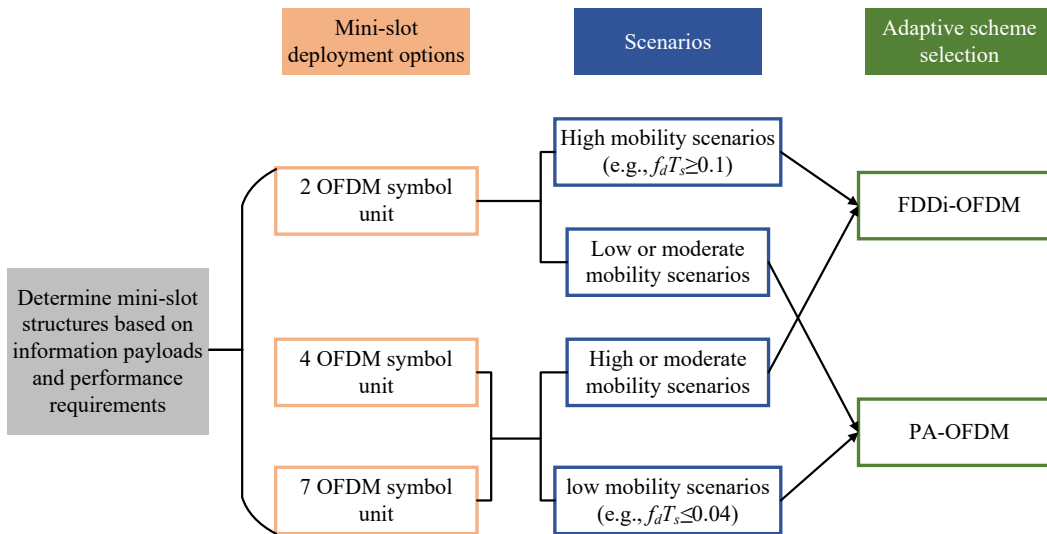


Fig. 8: Illustration of adaptive scheme selection for mini-slot-assisted SPT.

Doppler values. Specifically, the simulation parameters of Fig.7 are set to be consistent with that of Fig.6(b) and Fig.6(d), except $f_d T_s$. From Fig.7, the analytical and simulated BLER of FDDi-OFDM stays constant with the increase of $f_d T_s$. This is because, for FDDi-OFDM, data detection is only affected by received signals over two adjacent sub-carriers, which is independent of channel variation over two adjacent OFDM symbols. It is also seen that the BLER of PA-OFDM is better than that of FDDi-OFDM, when $f_d T_s$ is small. However, when $f_d T_s$ increases to a certain value, the BLER performance of PA-OFDM becomes worse than that of FDDi-OFDM. As a result, we can adaptively activate or switch between PA-OFDM and FDDi-OFDM to achieve efficient URLLC based on information payloads, mini-slot deployment options, user mobility, and service requirements, as illustrated in Fig.8.

V. CONCLUSIONS

In this paper, we have proposed an adaptive scheme that integrates both differential and coherent detection for mini-slot-assisted short packet URLLC, effectively balancing training overhead, reliability, and latency performance. To evaluate the performance of the proposed schemes, we derived the BLER performance using non-asymptotic information-theoretic bounds. The simulation results verified the accuracy of the analysis and showed the feasibility and effectiveness of adaptive differential and coherent detection.

The results of this paper are based on single BS association (i.e. single connection). One further issue is the impact of multi-BS association (i.e. macro diversity), which we are currently investigating.

APPENDIX A: PROOF OF THEOREM 3

For convenience, we take FDDi-OFDM as an example and the performance analytical results of TDDi-OFDM can be obtained following similar steps. The proof consists of the four steps below.

Step 1. Equivalent representation of DM: For ease of utilizing the non-asymptotic information-theoretic bounds in Theorem 1 and 2 to evaluate the SPT performance, we first give an equivalent representation of DM. Since DM uses the phase difference between two consecutive symbols to transmit information, we, without loss of generality, assume that the phases of the input data $v_{k,t}$ and symbol $d_{k-1,t}$ in (1) are $\Delta\varphi$ and φ , respectively. Thus, the complex representation of the transmitted symbol $d_{k,t}$ in (1) is $e^{j(\varphi+\Delta\varphi)}$. Based on (12), the corresponding received signal of $d_{k-1,t}$ and $d_{k,t}$ can be rewritten as

$$\begin{cases} z_{k-1,t} = H_{k-1,t} e^{j\varphi} + W_{k-1,t} \\ z_{k,t} = H_{k,t} e^{j(\varphi+\Delta\varphi)} + W_{k,t} \end{cases} \quad (37)$$

Furthermore, we decompose the complex random variables $z_{k-1,t}$, $z_{k,t}$, $W_{k-1,t}$ and $W_{k,t}$ of (37) into their real and imaginary parts:

$$\begin{cases} z_{k-1,t} = x_1 + jy_1 \\ z_{k,t} = x_2 + jy_2 \\ W_{k-1,t} = w_{r,1} + jw_{i,1} \\ W_{k,t} = w_{r,2} + jw_{i,2} \end{cases}$$

Let r_1 , ϕ_1 , r_2 and ϕ_2 be the amplitude and phase factors of $H_{k-1,t}$ and $H_{k,t}$, respectively. Then, we have

$$\begin{cases} x_1 = r_1 \cos \theta_1 + w_{r,1} \\ y_1 = r_1 \sin \theta_1 + w_{i,1} \\ x_2 = r_2 \cos (\theta_2 + \Delta\varphi) + w_{r,2} \\ y_2 = r_2 \sin (\theta_2 + \Delta\varphi) + w_{i,2} \end{cases} \quad (38)$$

where $\theta_1 = \phi_1 + \varphi$ and $\theta_2 = \phi_2 + \varphi$. Note that since ϕ_1 and ϕ_2 are uniformly distributed on $[0, 2\pi]$ for WSSUS Rayleigh fading channels, θ_1 and θ_2 are also uniformly distributed on $[0, 2\pi]$. Let $\mathbf{z} = \{x_1, y_1, x_2, y_2\}$. As expressed in (38), DM can be equivalently described by the conditional transition probability $\mathbb{P}_{\mathbf{z}|\Delta\varphi}$ with the channel input $\Delta\varphi$ and the channel

output \mathbf{z} . This equivalent representation of DM in (38) makes tractable the channel transition probability and information density in Theorems 1 and 2.

Step 2. Conditional channel transition probability $\mathbb{P}_{\mathbf{z}|\Delta\varphi}$ of (38): From (38), we obtain

$$\begin{cases} \mathbb{E}\{x_1x_2\} = \eta_f \cos \Delta\varphi \\ \mathbb{E}\{x_1y_2\} = \eta_f \sin \Delta\varphi \\ \mathbb{E}\{y_1x_2\} = -\eta_f \sin \Delta\varphi \\ \mathbb{E}\{y_1y_2\} = \eta_f \cos \Delta\varphi \end{cases}$$

for FDDi-OFDM, where $\eta_f = \rho_f/2$ and ρ_f is the frequency domain correlation defined in (8). In addition, since x_1, y_1, x_2, y_2 are a set of zero-mean Gaussian random variables with variances $\sigma^2 = (1 + \gamma)/(2\gamma)$, the covariance matrix of \mathbf{z} is given by

$$\Sigma = \begin{bmatrix} \sigma^2 & 0 & \eta_f \cos \Delta\varphi & \eta_f \sin \Delta\varphi \\ 0 & \sigma^2 & -\eta_f \sin \Delta\varphi & \eta_f \cos \Delta\varphi \\ \eta_f \cos \Delta\varphi & -\eta_f \sin \Delta\varphi & \sigma^2 & 0 \\ \eta_f \sin \Delta\varphi & \eta_f \cos \Delta\varphi & 0 & \sigma^2 \end{bmatrix} \quad (39)$$

Based on (39), we have $|\Sigma| = (\sigma^4 - \eta_f^2)^2$ and

$$\Sigma^{-1} = \frac{1}{\sigma^4 - \eta_f^2} \times \begin{bmatrix} \sigma^2 & 0 & -\eta_f \cos \Delta\varphi & -\eta_f \sin \Delta\varphi \\ 0 & \sigma^2 & \eta_f \sin \Delta\varphi & -\eta_f \cos \Delta\varphi \\ -\eta_f \cos \Delta\varphi & \eta_f \sin \Delta\varphi & \sigma^2 & 0 \\ -\eta_f \sin \Delta\varphi & -\eta_f \cos \Delta\varphi & 0 & \sigma^2 \end{bmatrix}$$

As a result, the conditional channel transition probability $\mathbb{P}_{\mathbf{z}|\Delta\varphi}$ of (38) can be expressed as

$$\begin{aligned} \mathbb{P}_{\mathbf{z}|\Delta\varphi}(x_1, y_1, x_2, y_2 | \Delta\varphi) &= \frac{\exp(-\frac{1}{2}\mathbf{z}\Sigma^{-1}\mathbf{z}^T)}{\sqrt{16\pi^4 |\Sigma|}} \\ &= \frac{1}{4\pi^2 (\sigma^4 - \eta_f^2)} \exp\left[\frac{\eta_f \mathcal{F}(\Delta\varphi)}{2(\sigma^4 - \eta_f^2)}\right] \times \\ &\exp\left[-\frac{(\sigma^2 + \eta_f)(x_1^2 + y_1^2 + x_2^2 + y_2^2)}{2(\sigma^4 - \eta_f^2)}\right] \\ &= \frac{\gamma^2}{\pi^2 (1 + 2\gamma + \gamma^2 - \gamma^2 \rho_f^2)} \exp\left[\frac{\gamma^2 \rho_f \mathcal{F}(\Delta\varphi)}{1 + 2\gamma + \gamma^2 - \gamma^2 \rho_f^2}\right] \times \\ &\exp\left[-\frac{\gamma(1 + \gamma + \gamma \rho_f)(x_1^2 + y_1^2 + x_2^2 + y_2^2)}{1 + 2\gamma + \gamma^2 - \gamma^2 \rho_f^2}\right] \end{aligned} \quad (40)$$

where $\mathcal{F}(\Delta\varphi) = (x_1 + x_2 \cos \Delta\varphi + y_2 \sin \Delta\varphi)^2 + (y_1 - x_2 \sin \Delta\varphi + y_2 \cos \Delta\varphi)^2$

Step 3. Expectation and variance of the information density for (38): Based on (20) and (40), we can calculate the expectation and variance of the information density for (38). Both are key parameters to describe the asymptotic behavior of the non-asymptotic upper and lower bounds in Theorems 1 and 2, as shown next in Step 4. According to the definition

in (20), the information density for (38) with a single channel use is

$$i(\Delta\varphi; \mathbf{z}) = \log_2 \frac{\mathbb{P}_{\mathbf{z}|\Delta\varphi}(x_1, y_1, x_2, y_2 | \Delta\varphi)}{\mathbb{P}_{\mathbf{z}}(x_1, y_1, x_2, y_2)}. \quad (41)$$

Then, the expectation and variance of $i(\Delta\varphi; \mathbf{z})$ can be respectively determined as

$$\begin{aligned} I_{\text{diff}}(\gamma) &= \mathbb{E}[i(\Delta\varphi; \mathbf{z})] \\ &= \log_2 M - \mathbb{E}\left\{\log_2 \frac{\sum_{m=0}^{M-1} \mathbb{P}_{\mathbf{z}|\Delta\varphi_m}(x_1, y_1, x_2, y_2 | \Delta\varphi_m)}{\mathbb{P}_{\mathbf{z}|\Delta\varphi_0}(x_1, y_1, x_2, y_2 | \Delta\varphi_0)}\right\} \\ &= \log_2 M - \mathbb{E}\left\{\log_2 \frac{\sum_{m=0}^{M-1} \exp\left[\frac{\gamma^2 \rho_f \mathcal{F}(\Delta\varphi_m)}{1 + 2\gamma + \gamma^2 - \gamma^2 \rho_f^2}\right]}{\exp\left[\frac{\gamma^2 \rho_f \mathcal{F}(\Delta\varphi_0)}{1 + 2\gamma + \gamma^2 - \gamma^2 \rho_f^2}\right]}\right\} \end{aligned} \quad (42)$$

and

$$\begin{aligned} V_{\text{diff}}(\gamma) &= \text{Var}[i(\Delta\varphi; \mathbf{z})] \\ &= \mathbb{E}\left\{\left[\log_2 \frac{\sum_{m=0}^{M-1} \mathbb{P}_{\mathbf{z}|\Delta\varphi_m}(x_1, y_1, x_2, y_2 | \Delta\varphi_m)}{\mathbb{P}_{\mathbf{z}|\Delta\varphi_0}(x_1, y_1, x_2, y_2 | \Delta\varphi_0)}\right]^2\right\} \\ &\quad - \mathbb{E}^2\left\{\log_2 \frac{\sum_{m=0}^{M-1} \mathbb{P}_{\mathbf{z}|\Delta\varphi_m}(x_1, y_1, x_2, y_2 | \Delta\varphi_m)}{\mathbb{P}_{\mathbf{z}|\Delta\varphi_0}(x_1, y_1, x_2, y_2 | \Delta\varphi_0)}\right\} \\ &= \mathbb{E}\left\{\left[\log_2 \frac{\sum_{m=0}^{M-1} \exp\left[\frac{\gamma^2 \rho_f \mathcal{F}(\Delta\varphi_m)}{1 + 2\gamma + \gamma^2 - \gamma^2 \rho_f^2}\right]}{\exp\left[\frac{\gamma^2 \rho_f \mathcal{F}(\Delta\varphi_0)}{1 + 2\gamma + \gamma^2 - \gamma^2 \rho_f^2}\right]}\right]^2\right\} \\ &\quad - \mathbb{E}^2\left\{\log_2 \frac{\sum_{m=0}^{M-1} \exp\left[\frac{\gamma^2 \rho_f \mathcal{F}(\Delta\varphi_m)}{1 + 2\gamma + \gamma^2 - \gamma^2 \rho_f^2}\right]}{\exp\left[\frac{\gamma^2 \rho_f \mathcal{F}(\Delta\varphi_0)}{1 + 2\gamma + \gamma^2 - \gamma^2 \rho_f^2}\right]}\right\} \end{aligned} \quad (43)$$

where $\Delta\varphi_m = 2\pi m/M$.

Step 4. Normal approximation for the IS and DT Bounds in Theorems 1 and 2: Based on $I_{\text{diff}}(\gamma)$ in (42) and $V_{\text{diff}}(\gamma)$ in (43), the normal approximation results can be finally obtained by using the derivation techniques in [39, Appendix A] and [43]. ■

REFERENCES

- [1] 3GPP, "Service requirements for the 5G system," TS 22.261 V19.5.0., Release 19, Dec. 2023.
- [2] 3GPP, "Study on physical layer enhancements for NR ultra-reliable and low latency case (URLLC)," TR 38.824 V16.0.0., Release 16, Mar. 2019.
- [3] C.-X. Wang *et al.*, "On the road to 6G: visions, requirements, key technologies, and testbeds," *IEEE Commun. Surveys & Tutorials*, vol. 25, no. 2, pp. 905–974, Secondquarter 2023.
- [4] X. You *et al.*, "Towards 6G wireless communication networks: vision, enabling technologies, and new paradigm shifts," *Sci. China Inf. Sci.*, vol. 64, pp. 1–74, Jan. 2021, doi:10.1007/s11432-020-2955-6.
- [5] C. She *et al.*, "A tutorial of ultra-reliable and low-latency communications in 6G: Integrating domain knowledge into deep learning," *Proc. IEEE*, vol. 109, no. 3, pp. 204–246, Mar. 2021.
- [6] 3GPP, "Study on new radio (NR) access technology," TR 38.912 V17.0.0., Release 17, Mar. 2022.
- [7] 3GPP, "Physical channels and modulation," TS 38.211 V18.1.0., Release 18, Dec. 2023.
- [8] D. Feng *et al.*, "Towards Ultra-Reliable Low-Latency Communications: Typical Scenarios, Possible Solutions, and Open Issues," *IEEE Veh. Technol. Mag.*, vol. 14, no. 2, pp. 94–102, June 2019.
- [9] G. Durisi, T. Koch, and P. Popovski, "Toward massive, ultrareliable, and low-latency wireless communication with short packets," *Proc. IEEE*, vol. 104, no. 9, pp. 1711–1726, Sept. 2016.

- [10] C. Xu *et al.*, "Sixty years of coherent versus non-coherent tradeoffs and the road from 5G to wireless futures," *IEEE Access*, vol. 7, pp. 178 246–178 299, Dec. 2019.
- [11] L. Wang and L. Hanzo, "Dispensing with channel estimation: Differentially modulated cooperative wireless communications," *IEEE Commun. Surveys & Tutorials*, vol. 14, no. 3, pp. 836–857, 2012.
- [12] V. M. Baeza and A. G. Armada, "Non-coherent massive SIMO system based on M-DPSK for rician channels," *IEEE Trans. on Veh. Technol.*, vol. 68, no. 3, pp. 2413–2426, Mar. 2019.
- [13] M. R. Avendi *et al.*, "Performance of selection combining for differential amplify-and-forward relaying over time-varying channels," *IEEE Trans. on Wireless Commun.*, vol. 13, no. 8, pp. 4156–4166, Aug. 2014.
- [14] T. Himsoon *et al.*, "Differential modulations for multinode cooperative communications," *IEEE Trans. on Signal Process.*, vol. 56, no. 7, pp. 2941–2956, July 2008.
- [15] K. Zhong *et al.*, "A general SER formula for an OFDM system with MDPSK in frequency domain over rayleigh fading channels," *IEEE Trans. on Commun.*, vol. 52, no. 4, pp. 584–594, Apr. 2004.
- [16] S. Osaki, M. Nakao, T. Ishihara, and S. Sugiura, "Differentially modulated spectrally efficient frequency-division multiplexing," *IEEE Signal Process. Lett.*, vol. 26, no. 7, pp. 1046–1050, Jul. 2019.
- [17] Y. Polyanskiy and S. Verdú, "Scalar coherent fading channel: Dispersion analysis," in *Proc. IEEE Int. Symp. on Inf. Theory*, 2011, pp. 2959–2963.
- [18] A. Collins and Y. Polyanskiy, "Coherent multiple-antenna block-fading channels at finite blocklength," *IEEE Trans. on Inf. Theory*, vol. 65, no. 1, pp. 380–405, Jan. 2019.
- [19] W. Yang, G. Durisi, T. Koch, and Y. Polyanskiy, "Quasi-static multiple-antenna fading channels at finite blocklength," *IEEE Trans. on Inf. Theory*, vol. 60, no. 7, pp. 4232–4265, July 2014.
- [20] G. C. Ferrante *et al.*, "Pilot-assisted short-packet transmission over multi-antenna fading channels: A 5G case study," in *Proc. IEEE Conf. on Inf. Sci. and Syst. (CISS)*, Mar. 2018, pp. 1–6.
- [21] A. O. Kislal *et al.*, "Efficient evaluation of the error probability for pilot-assisted URLLC with massive MIMO," *IEEE J. on Sel. Areas in Commun.*, vol. 41, no. 7, pp. 1969–1981, July 2023.
- [22] J. Östman, A. Lancho, G. Durisi, and L. Sanguinetti, "URLLC with massive MIMO: Analysis and design at finite blocklength," *IEEE Trans. on Wireless Commun.*, vol. 20, no. 10, pp. 6387–6401, Oct. 2021.
- [23] A. Lancho, G. Durisi, and L. Sanguinetti, "Cell-free massive MIMO for URLLC: A finite-blocklength analysis," *IEEE Trans. on Wireless Commun.*, vol. 22, no. 12, pp. 8723–8735, Dec. 2023.
- [24] M. Mousaei and B. Smida, "Optimizing pilot overhead for ultra-reliable short-packet transmission," in *Proc. IEEE Conf. Commun. (ICC)*, May 2017, pp. 1–5.
- [25] J. Cao *et al.*, "Independent pilots versus shared pilots: Short frame structure optimization for heterogeneous-traffic urllc networks," *IEEE Trans. on Wireless Commun.*, vol. 21, no. 8, pp. 5755–5769, Aug. 2022.
- [26] X. Zhou *et al.*, "Joint optimization of frame structure and power allocation for URLLC in short blocklength regime," *IEEE Trans. on Commun.*, vol. 71, no. 12, pp. 7333–7346, Dec. 2023.
- [27] B. Lee *et al.*, "Packet structure and receiver design for low latency wireless communications with ultra-short packets," *IEEE Trans. on Commun.*, vol. 66, no. 2, pp. 796–807, Feb. 2018.
- [28] J. Östman *et al.*, "Short packets over block-memoryless fading channels: Pilot-assisted or noncoherent transmission?" *IEEE Trans. on Commun.*, vol. 67, no. 2, pp. 1521–1536, Feb. 2019.
- [29] A. Lancho, T. Koch, and G. Durisi, "On single-antenna rayleigh block-fading channels at finite blocklength," *IEEE Trans. on Inf. Theory*, vol. 66, no. 1, pp. 496–519, Jan. 2020.
- [30] A. Lancho *et al.*, "Saddlepoint approximations for short-packet wireless communications," *IEEE Trans. on Wireless Commun.*, vol. 19, no. 7, pp. 4831–4846, Jul. 2020.
- [31] C. Qi and T. Koch, "A high-SNR normal approximation for MIMO rayleigh block-fading channels," in *Proc. IEEE Int. Symp. on Inf. Theory*, 2020, pp. 2314–2319.
- [32] J. Wu, W. Kim, and B. Shim, "Pilot-less one-shot sparse coding for short packet-based machine-type communications," *IEEE Trans. on Veh. Technol.*, vol. 69, no. 8, pp. 9117–9120, Aug. 2020.
- [33] H. Ji, W. Kim, and B. Shim, "Pilot-less sparse vector coding for short packet transmission," *IEEE Wireless Commun. Lett.*, vol. 8, no. 4, pp. 1036–1039, Aug. 2019.
- [34] Y. Liu *et al.*, "Fast iterative semi-blind receiver for URLLC in short-frame full-duplex systems with CFO," *IEEE J. on Sel. Areas in Commun.*, vol. 37, no. 4, pp. 839–853, Apr. 2019.
- [35] P. Walk, P. Jung, and B. Hassibi, "MOCZ for blind short-packet communication: Basic principles," *IEEE Trans. on Wireless Commun.*, vol. 18, no. 11, pp. 5080–5097, Nov. 2019.
- [36] A. A. Siddiqui *et al.*, "Spectrally-efficient modulation on conjugate-reciprocal zeros (SE-MOCZ) for non-coherent short packet communications," *IEEE Trans. on Wireless Commun.*, vol. 23, no. 3, pp. 2226–2240, Mar. 2024.
- [37] J. Choi and N. Lee, "Generalized differential index modulation for pilot-free communications," *IEEE Internet of Things J.*, vol. 8, no. 10, pp. 7973–7984, May 2021.
- [38] X. Jiang *et al.*, "Packet detection by a single OFDM symbol in URLLC for critical industrial control: A realistic study," *IEEE J. on Sel. Areas in Commun.*, vol. 37, no. 4, pp. 933–946, Apr. 2019.
- [39] C. Zheng *et al.*, "Differential modulation for short packet transmission in URLLC," *IEEE Trans. on Wireless Commun.*, vol. 23, no. 7, pp. 7230–7245, Jul. 2024.
- [40] D.-B. Lin *et al.*, "Performance of noncoherent maximum-likelihood sequence detection for differential OFDM systems with diversity reception," *IEEE Trans. on Broadcast.*, vol. 52, no. 1, pp. 62–70, Mar. 2006.
- [41] Y. Liu *et al.*, "Channel estimation for OFDM," *IEEE Commun. Surveys & Tutorials*, vol. 16, no. 4, pp. 1891–1908, Fourthquarter 2014.
- [42] J. Kim, J. Park, and D. Hong, "Performance analysis of channel estimation in OFDM systems," *IEEE Signal Process. Lett.*, vol. 12, no. 1, pp. 60–62, Jan. 2005.
- [43] Y. Polyanskiy, H. V. Poor, and S. Verdú, "Channel coding rate in the finite blocklength regime," *IEEE Trans. on Inf. Theory*, vol. 56, no. 5, pp. 2307–2359, May 2010.
- [44] E. MolavianJazi and J. N. Laneman, "A second-order achievable rate region for gaussian multi-access channels via a central limit theorem for functions," *IEEE Trans. on Inf. Theory*, vol. 61, no. 12, pp. 6719–6733, Dec. 2015.
- [45] Q. Xiong *et al.*, "Status prediction and data aggregation for AoI-oriented short-packet transmission in industrial IoT," *IEEE Trans. on Commun.*, vol. 71, no. 1, pp. 611–625, Jan. 2023.
- [46] C. Zheng *et al.*, "Open-loop communications for up-link URLLC under clustered user distribution," *IEEE Trans. on Veh. Technol.*, vol. 70, no. 11, pp. 11 509–11 522, Nov. 2021.
- [47] E. MolavianJazi, *A Unified Approach to Gaussian Channels with Finite Blocklength*. Ph.D. dissertation, Dept. Elect. Eng., Univ. Notre Dame, Notre Dame, IN, USA, July 2014.
- [48] R. M. Rao, V. Marojevic, and J. H. Reed, "Adaptive pilot patterns for CA-OFDM systems in nonstationary wireless channels," *IEEE Trans. on Veh. Technol.*, vol. 67, no. 2, pp. 1231–1244, Feb. 2018.
- [49] M. Šimko *et al.*, "Adaptive pilot-symbol patterns for MIMO OFDM systems," *IEEE Trans. on Wireless Commun.*, vol. 12, no. 9, pp. 4705–4715, Sep. 2013.
- [50] O. Edfors *et al.*, "OFDM channel estimation by singular value decomposition," *IEEE Trans. on Commun.*, vol. 46, no. 7, pp. 931–939, Jul. 1998.
- [51] P. Yuan *et al.*, "Polar-coded non-coherent communication," *IEEE Commun. Lett.*, vol. 25, no. 6, pp. 1786–1790, Feb. 2021.